INTERNATIONAL JOURNAL FOR NUMERICAL METHODS IN FLUIDS
Int. J. Numer. Meth. Fluids 2006; **50**:1357–1368
Published online 10 February 2006 in Wiley InterScience (www.interscience.wiley.com). DOI: 10.1002/fld.1193

Volumetric methods for evaluating irreversible energy losses and entropy production with application to bioengineering flows

Keri Moyle[1,‡], Gordon Mallinson[1,*,†] and Brett Cowan[2,§]

[1]*Department of Mechanical Engineering, University of Auckland, Auckland, New Zealand*
[2]*Centre for Advanced MRI, University of Auckland, Auckland, New Zealand*

SUMMARY

Methods for calculating irreversible energy losses and rates of heat transfer from computational fluid dynamics solutions using volume integrations of energy dissipation functions contrast with the more usual approach of performing first law energy balances over the boundaries of a flow domain. Advantages of the approach are that the estimates involve the whole flow domain, and are hence based on more information than would otherwise be used, and that the energy dissipation function allows for detailed assessment of the mechanisms and regions of energy loss.

The research was motivated by a need to clarify energy losses by haemodynamics in the greater vessels of the human body, in particular, the Fontan connection. For this application irreversible energy losses were calculated using the viscous dissipation function. Streamwise integration of the viscous dissipation function is also used to explore the ways in which different flow structures contribute to energy losses. Copyright © 2006 John Wiley & Sons, Ltd.

KEY WORDS: irreversible losses; viscous dissipation; Fontan connection; bioengineering; computational fluid dynamics; total cavopulmonary connection

INTRODUCTION

This research was motivated by a study of bioengineering flows where it was important to estimate the work required to pump blood through connections in arterial systems. For example, a 'Fontan connection' is the result of a palliative operation used to treat severe congenital heart defects, by re-routing blood through an interconnecting conduit to bypass a

*Correspondence to: G. Mallinson, Department of Mechanical Engineering, University of Auckland, Private Bag 92019, Auckland, New Zealand.
†E-mail: g.mallinson@auckland.ac.nz
‡E-mail: keri.moyle@eng.ox.ac.uk
§E-mail: b.cowan@auckland.ac.nz

Contract/grant sponsor: National Heart Foundation of New Zealand

Received 15 March 2005
Revised 3 November 2005
Accepted 26 December 2005

defective or inoperative ventricle. The geometry of a typical connection is shown in Figure 1 and the description here is relevant for a deficient right ventricle which pumps blood returning from below (via the inferior vena cava, IVC) and above (via the superior vena cava, SVC) the heart to the lungs (via the left and right pulmonary arteries). Early operations that included the right atrium (the chamber ordinarily connecting the IVC and SVC to the ventricle) are called atriopulmonary connections, while modern operations that do not include the atrium are called total cavopulmonary connections. The computer model in Figure 1 represents an atriopulmonary connection.

The design objectives for Fontan connections are to ensure balanced flows to the lungs, to minimize flow work losses and to circumvent flow characteristics known to lead to blood clotting and other detrimental effects [1, 2]. The absence of the pulmonary ventricle means that the remaining systemic ventricle must carry the load of the whole circulation system. It is therefore important to design a connection to minimize energy loss.

The conventional approach (e.g. References [3–6]) for estimating the energy lost in a connection is to place a control volume around it and perform momentum and energy balances. There are two main issues with this approach. The first is that it may be difficult to distinguish the irreversible and reversible losses, the former being the major factor in determining the impact the connection has on the system efficiency. The second is that the calculations are performed on the boundaries, in this case the inlets and outlets of the connection, and no information regarding the ways that the internal flow structures individually lose energy is obtained.

An alternative approach is to estimate the irreversible losses directly. In a Fontan connection, or any other flow for that matter, energy is lost irreversibly as the fluid works against viscosity. This loss can be represented as a volumetric energy sink by the viscous dissipation function.

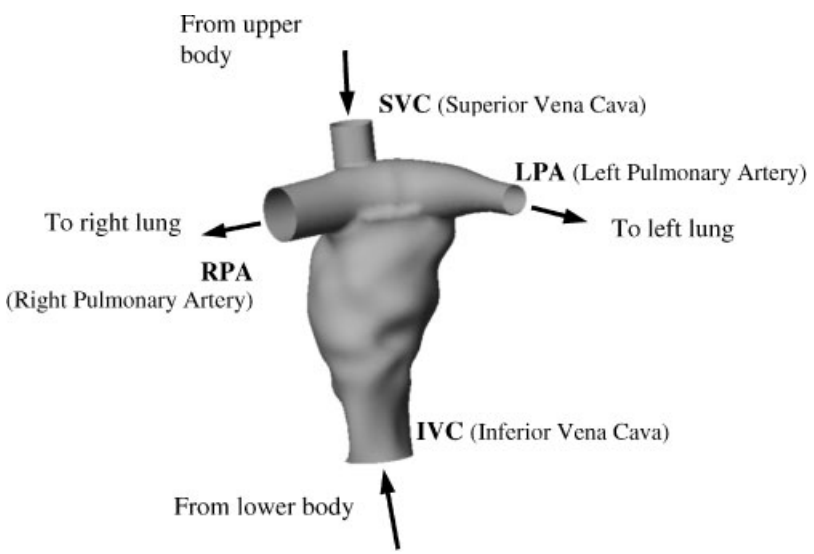

Figure 1. The geometry of and flow through a Fontan connection. This is a patient-specific model of an atriopulmonary connection that includes the right atrium.

This is appropriate, even if the flow can be regarded as being isothermal. The fact that the viscous dissipation is not a significant factor in the energy equation means that it does not significantly influence the distribution of specific enthalpy in the fluid. It can, however, be important for the production of entropy, and hence the viscous dissipation function is useful for the estimation of irreversible energy losses. The utility of the viscous dissipation function for estimating overall energy losses in biomedical flows has already been recognized [7]. However, it does not appear to have been used to elucidate the details of how the energy losses are distributed in a connection.

METHODS

Assumptions and governing equations. For this study the fluid is assumed to be Newtonian, to have constant properties and to be incompressible. Equations (1) and (2) are the relevant versions of the momentum and energy equations, respectively. The only departure from the usual treatment of such flows is the inclusion of the viscous dissipation term in the energy equation.

$$\frac{\mathrm{D}\mathbf{u}}{\mathrm{D}t} = -\frac{\nabla P}{\rho} + \nu\nabla^2\mathbf{u} \tag{1}$$

$$\frac{\mathrm{D}T}{\mathrm{D}t} = \frac{k}{\rho c_p}\nabla^2 T + \frac{\nu}{c_p}\Phi \tag{2}$$

The function Φ is the viscous dissipation function which for a three-dimensional Cartesian coordinate system has the form,

$$\Phi = 2\left\{\left(\frac{\partial u}{\partial x}\right)^2 + \left(\frac{\partial v}{\partial y}\right)^2 + \left(\frac{\partial w}{\partial z}\right)^2\right\} + \left(\frac{\partial v}{\partial x} + \frac{\partial u}{\partial y}\right)^2 + \left(\frac{\partial w}{\partial y} + \frac{\partial v}{\partial z}\right)^2 + \left(\frac{\partial u}{\partial z} + \frac{\partial w}{\partial x}\right)^2 \tag{3}$$

In a two-dimensional coordinate system Φ reduces to

$$\Phi = 2\left\{\left(\frac{\partial u}{\partial x}\right)^2 + \left(\frac{\partial v}{\partial y}\right)^2\right\} + \left(\frac{\partial v}{\partial x} + \frac{\partial u}{\partial y}\right)^2 \tag{4}$$

Scaling and nondimensional equations. The equations can be written in nondimensional forms by choosing appropriate reference quantities for all the variables in the governing equations. Equations (5) and (6) are the result of choosing a single characteristic length L, a reference velocity U_{ref}, using ρU_{ref}^2 as a reference for pressure and representing the absolute temperature by $T = T_0 + \Delta T\theta$.

$$\frac{\mathrm{D}\mathbf{u}}{\mathrm{D}t} = -\nabla P + \frac{1}{Re}\nabla^2\mathbf{u} \tag{5}$$

$$\frac{\mathrm{D}\theta}{\mathrm{D}t} = \frac{1}{Pe}[\nabla^2\theta + Ec\,Pr\Phi] \tag{6}$$

Conventional practice is followed, whereby it is understood that the variables appearing in equations containing nondimensional numbers have been scaled whereas those containing

dimensional parameters have not. The product $Ec\,Pr$, which indicates the relative strength of viscous dissipation to conduction in the transport of energy is called the Brinkmann number.

Viscous dissipation and a control volume energy balance. For many common flow situations the Brinkmann number is small and the viscous dissipation function can be dropped from Equation (6). This means that the flow and temperature fields are not influenced by the heat released as work is done against viscosity. The energy is, nevertheless, lost irreversibly from the fluid and the rate of loss can be estimated by integrating the viscous dissipation function over the volume occupied by the fluid.

$$\dot{Q}_{\text{irrev}} = \mu \int_V \Phi \, \mathrm{d}v \tag{7}$$

For an open control volume surrounding a steady flow the conservation of energy can be expressed as,

$$\dot{Q} - \dot{W} = \Delta \dot{E} \tag{8}$$

where $\dot{Q}$ is the heat transfer into the volume, $\dot{W}$ is the rate of work done by the fluid on its surroundings, and $\Delta \dot{E}$ and is the total rate at which energy leaves the volume. For the processes considered here, $\Delta \dot{E}$ is a summation over all openings of the outward energy flow rates.

The rate of heat generation by viscous dissipation, $\dot{Q}_{\text{irrev}}$, is eventually transferred across the boundaries and is lost by the fluid. It is therefore a negative contribution to $\dot{Q}$ in Equation (8).

Energy loss calculation. The connection can be enclosed by an open control volume. The relevant version of Equation (8) is

$$\dot{Q} - \dot{W} = \sum_{\text{outlets}} \dot{m}(h + \tfrac{1}{2}u^2) - \sum_{\text{inlets}} \dot{m}(h + \tfrac{1}{2}u^2) \tag{9}$$

where changes in potential energy have been neglected. There is no shaft work on the connection (since the walls are assumed here to be rigid). Recalling that the viscous dissipation eventually results in heat transfer from the control volume,

$$\dot{Q}_{\text{irrev}} = \sum_{\text{inlets}} \dot{m}(h + \tfrac{1}{2}\,u^2) - \sum_{\text{outlets}} \dot{m}(h + \tfrac{1}{2}u^2) \tag{10}$$

The specific enthalpy, $h = u + \frac{P}{\rho}$, at an inlet or outlet contains contributions from the internal energy and flow work. Conventional bioengineering analysis [3] assumes that the flow is isothermal so that the contribution from internal energy can be neglected. Equation (10) becomes

$$\dot{Q}_{\text{irrev}} = \sum_{\text{inlets}} \dot{V}(p + \tfrac{1}{2}\,\rho u^2) - \sum_{\text{outlets}} \dot{V}(p + \tfrac{1}{2}\,\rho u^2) \tag{11}$$

which can be used as an alternative to (7) for estimating the irreversible losses in a connection. In practice, Equation (11) is integrated over a cardiac cycle to give the total energy lost per cycle. To set a context for subsequent discussions, the power dissipated in a connection can be between 1 and 30 mW and the total flow rate approximately $5 \times 10^{-5}\ \mathrm{m}^3/\mathrm{s}$.

There is the philosophical issue of what happens to the heat generated by viscous dissipation in the connection. Locally, the internal energy of the fluid will be increased. Convection will carry the heated fluid downstream where the heat will eventually be transferred through the

vessel walls into the body. Strictly, or depending where the boundaries of the control volume are placed, the changes in internal energy should be accounted for in Equation (11). However, a first law analysis estimates that the influence of this heat on the temperature of the fluid is negligible. For example, given typical power dissipation and flow rates for a connection, the temperature of the blood will rise by around 10^{-6} K. It is therefore convenient to regard the flow as being isothermal and $\dot{Q}_{\text{irrev}}$ as the estimate of the rate of energy loss from the fluid.

NUMERICAL METHODS

CFD solver. The CFD system used to model the Fontan connections is an adaptation of MAC-like explicit methods to a collocated unstructured mesh that uses Voronoi cells as the control volumes [8]. Rhie-Chow interpolation is used and the convection approximations are Voronoi mesh adaptations of the ULTRA-QUICKEST scheme [9].

Method of model creation. Patient-specific CFD models were created from magnetic resonance images (MRI) that included anatomical and velocity information. The anatomical data were used to create a boundary tessellation that represented the connection. The tessellation was then used to generate a Voronoi mesh. It was not practicable to vary the boundary definition process in a way that led to meaningful parameterization, so the effects of errors in boundary definition were not explored.

The phase contrast (velocity) images that were used in this study had 1 mm in plane resolution and were spaced 5 mm apart. Typical coverage of a total cavopulmonary connection is shown in Figure 2, which also shows the boundary mesh created from anatomical images. Scans were made over the whole cardiac cycle (with a 15% trigger window) and all three velocity components could be recovered from the phase contrast images (one for each component). The resulting four-dimensional data set was available for validation.

Boundary conditions. Velocity scans were also made at the inlets and outlets of a connection. The former were used to provide the unsteady boundary conditions for the CFD model. The solutions for the total cavopulmonary connection (Figures 1–3, 4(a), 5, 6) used these unsteady velocity boundary conditions. The solutions for the atriopulmonary connection (Figures 4(b), 7–9) used time averaged steady state representations of the inlet velocity boundary conditions.

The magnitudes of the flows through the inlets are best described by the volume flow rates. In the total cavopulmonary connection the time average flow rates were approximately

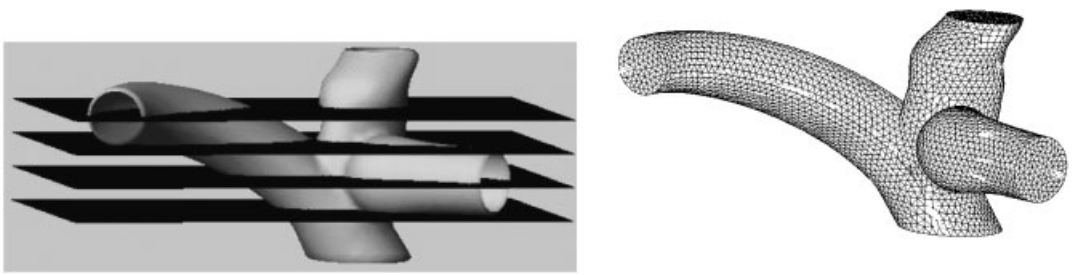

Figure 2. A total cavopulmonary connection showing scanning planes and a CFD mesh.

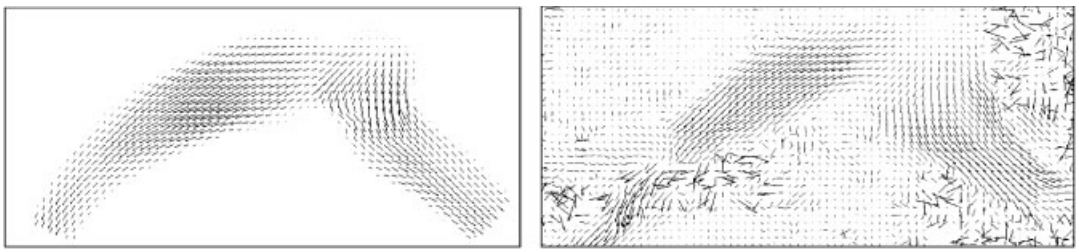

Figure 3. Comparison of the CFD and MRI velocity fields at the peak of the cardiac cycle in the second plane from the top of those in Figure 2. The CFD data have been sampled from the unstructured Voronoi mesh. The MRI data have been obtained from three-dimensional phase encoded images.

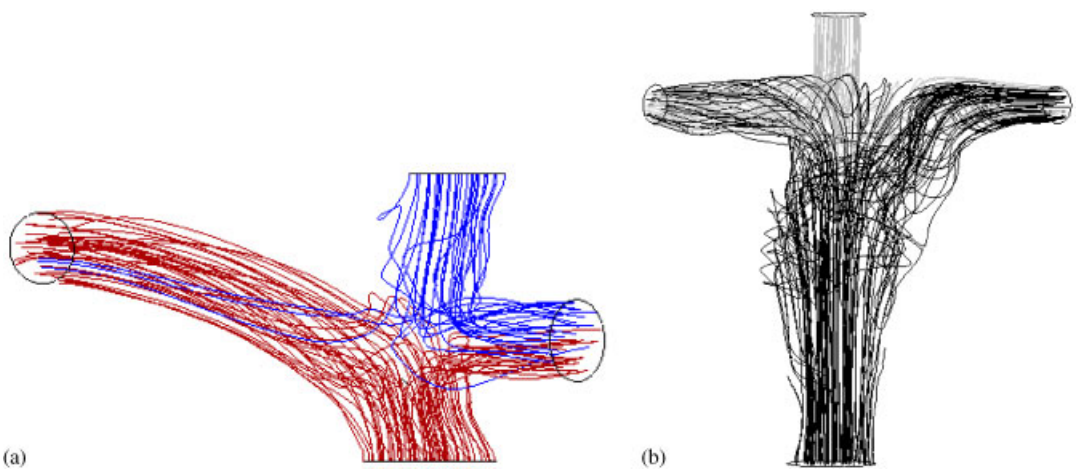

Figure 4. Streamlines in Fontan connections: (a) total cavopulmonary; and (b) atriopulmonary.

$1.2 \times 10^{-5}\,\mathrm{m}^3/\mathrm{s}$ through both the SVC and IVC. In the atriopulmonary connection the average flow rates through the inlets were $1 \times 10^{-5}\,\mathrm{m}^3/\mathrm{s}$.

The outlets from a connection had straight pipes added to them to place an outlet pressure boundary far from the exit to the connection. The measured division of flow between the two outlets was used to tune the CFD model by adjusting the outlet pressure boundary conditions, in order to represent the overall flow conditions in the connection and thereby generate comparable flow structures.

Verification and validation. The computational process was verified for a range of idealized test problems using a mesh refinement study [10] that confirmed second-order convergence. The results of a mesh refinement study for a Fontan model are summarized in Table I where the meshes number from 1 (most degrees of freedom) to 4 (least degrees of freedom). The coarsest mesh is clearly outside the range of monotonic convergence. Extrapolation assuming second-order convergence and based on any pair of the three finest meshes produced estimates

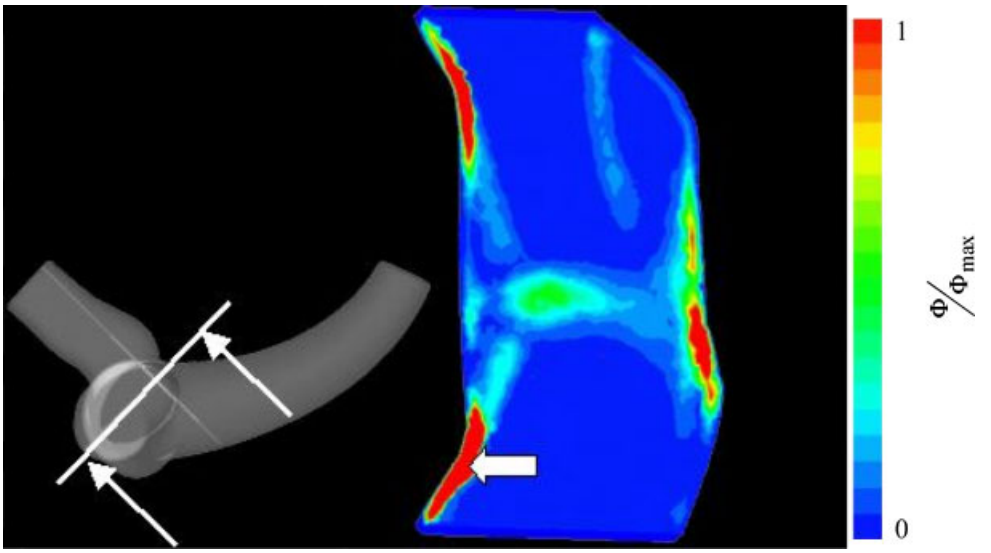

Figure 5. Map of viscous dissipation on a plane in a Fontan connection. The arrow on the contour map points the location of the peak in the dissipation function. The maximum value of Φ corresponds to a viscous dissipation rate of 3500 W/m^3.

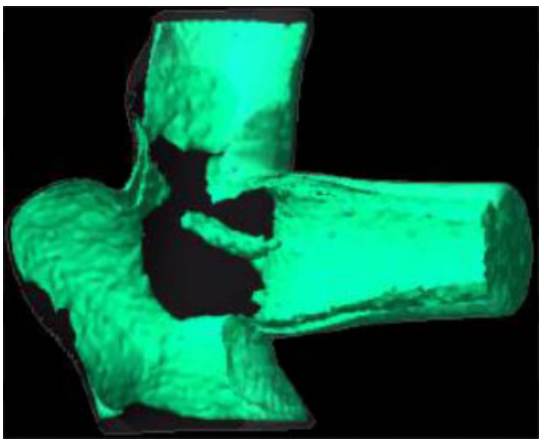

Figure 6. Iso-surface of viscous dissipation/unit volume ($\mu\Phi$) in a total cavopulmonary connection. The iso-surface level has been set to 350 W/m^3.

between 0.4096 and 0.4105 for the LPA mass flow fraction, indicating that the flow imbalance between the two pulmonary arteries is predicted to within 1% by the finest mesh.

Overall validation was possible by re-constituting the MRI measured flows from the CFD predictions. The velocity data were interpolated from the unstructured mesh onto regular grids that represented the sampling planes. An example of this comparison at the peak flow in the

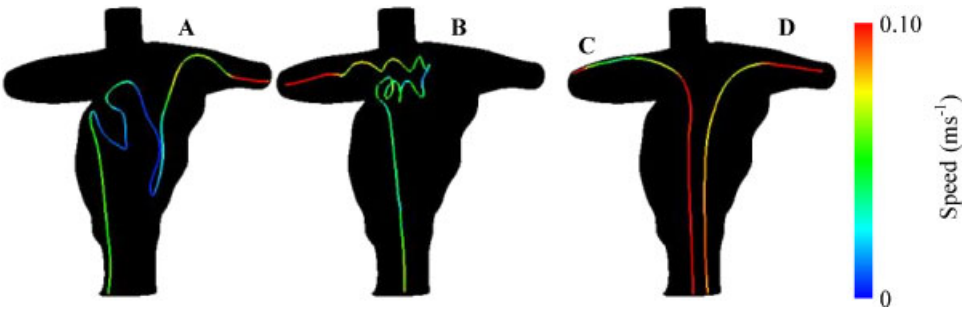

Figure 7. Streamlines representing flow categories in an atriopulmonary connection. Categories are: (A) large, slow recirculations; (B) small fast vortices; (C) near-wall streamline flow; and (D) mid-stream flow.

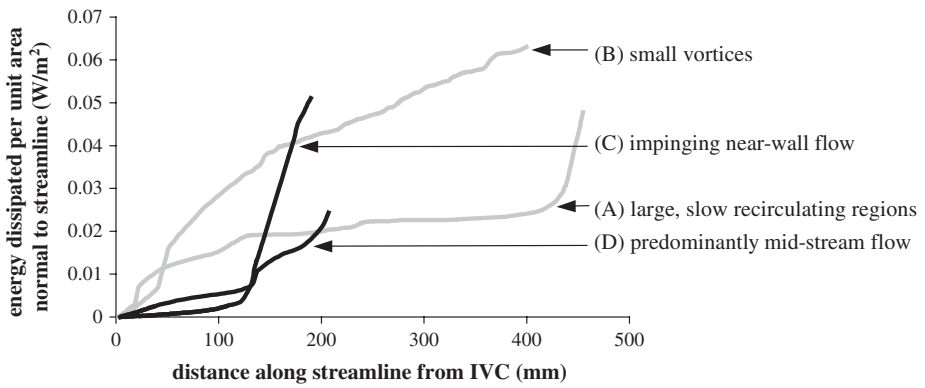

Figure 8. Cumulative energy dissipated along the streamlines in Figure 7.

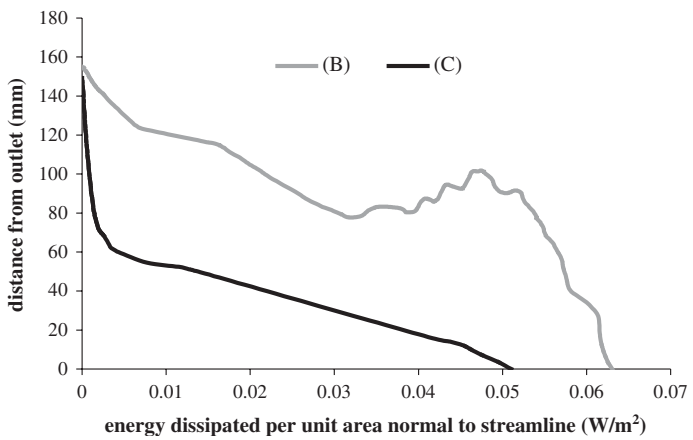

Figure 9. Goal-oriented analysis for streamlines B and C in Figure 7. The distance from the outlet is the straight-line distance from a point on a streamline to the outlet.

Table I. The influence of the mesh density on the left pulmonary artery mass flow fraction.

Mesh	1	2	3	4
Number of internal nodes	68 041	43 943	29 394	16 324
Number of boundary nodes	5522	4345	3368	2575
Average dimension	0.87	1.0	1.15	1.3225
LPA mass flow fraction	0.4121	0.4132	0.4140	0.4075

cardiac cycle is shown in Figure 3, for the second to top plane shown in Figure 2. The vectors are positioned at the locations sampled by the MRI system. The MRI data have not been processed to exclude measurements outside the connection, and the large apparently randomly directed vectors are in regions containing material, such as air in the lungs, which produce 'salt and pepper noise' when scanned.

Bearing in mind that the comparison in Figure 3 embraces the whole process of MRI measurement, image segmentation to create the models, boundary condition prescription and CFD modelling, it indicates that it is feasible to create CFD models that represent the overall characteristics of the flow. The validation process indicated that a key issue was the need to accurately describe the geometry of the connection, an issue exacerbated by the limited time that patients could be expected to remain in the scanner.

Numerical evaluation of viscous dissipation. Numerical evaluation of the viscous dissipation function relies on the evaluation of the velocity derivatives appearing in (3). In a three-dimensional Voronoi mesh there are typically 15 connections between any mesh point and its neighbours. The approximation to a derivative of any scalar ϕ is

$$\frac{\partial \phi}{\partial x} = \nabla \phi \cdot \mathbf{i} \approx \frac{\frac{1}{2}\sum_k \phi_k A_{i,k} \mathbf{n}_{i,k}}{V_i} \cdot \mathbf{i} \tag{12}$$

where i denotes the node in question and k a neighbour. $\mathbf{n}_{i,k}$ is the direction of the line between nodes i and k, and $A_{i,k}$ the area of the Voronoi face between them (which is always perpendicular to $\mathbf{n}_{i,k}$). The viscous dissipation function can be evaluated using expressions similar to (12) for the velocity gradients and then integrated over the domain to estimate the rate of irreversible energy loss.

RESULTS

Flow. A typical flow in a total cavopulmonary connection is indicated by the streamlines in Figure 4(a). There is a region of mixing where the streams collide. The streamlines are colour coded to indicate how the ascending and descending flows are eventually distributed between the pulmonary arteries. For example, in the total cavopulmonary connection the ascending blood is divided approximately equally between the pulmonary arteries, the descending flow is directed almost entirely to the left artery. Tracking streamlines in this way has utility for assessing the overall characteristics of a connection, as the formation of pulmonary atriovenous malformations is related to the distribution of flow from the liver between the lungs.

The streamlines for the atriopulmonary connection in Figure 4(b) show the more complex mixing flow in the atrium.

Irreversible energy loss. Attempts to apply Equation (11) to estimate the irreversible energy losses raised issues regarding integration over the boundaries of the Voronoi mesh to produce estimates for the terms in (11) that would accurately predict the losses, since these are quite small. The principle of integrating Φ to calculate an irreversible loss that compares favourably with (11) has already been demonstrated for a Fontan connection [7] and will not be pursued further here.

Distribution of viscous dissipation. For this application, the information provided by the viscous dissipation function proved to be more useful than the calculations of the overall energy loss. The variation of viscous dissipation function in a total cavopulmonary connection is shown by the plane slice contour map in Figure 5 and the iso-surface in Figure 6. The viscous dissipation is high in the shear layers adjacent to the walls. There is also a region of viscous dissipation where the flows collide and mix. The implications are that the regions of collision do lead to irreversible energy loss but the losses in the shear layers are at least an order of magnitude greater.

Losses along streamlines. Although the variation of Φ throughout the flow domain can lead to the identification of regions where losses occur, it does not necessarily indicate how the various kinds of flow contribute to the overall energy loss. The approach taken here was to compute the cumulative viscous energy dissipation along streamlines and is illustrated for the atriopulmonary connection. The four flow structures in Figure 7 were identified. These are large slow (<0.03 m/s) recirculations (A), rapid tight vortices (0.03–0.07 m/s) (B) and streamlined near the wall (C) and mid-stream (D) flow (>0.07 m/s).

Figure 8 shows the cumulative effect of the energy dissipated along the paths of the streamlines in Figure 7. The rates of energy loss are proportional to the slopes of the lines and the steepest slopes correspond to locations where streamlines approach or are in close proximity to the walls (e.g. C). Although the graphs in Figure 8 indicate the rate at which energy is lost along the streamlines, a better measure of the effect flow features have on the overall connection efficiency may be gained by assessing the energy losses against an appropriate objective. The purpose of the connection is to allow blood to pass through it with minimal loss of energy. The streamlines in Figure 7 indicate that this can be accomplished by a variety of paths of differing lengths. The length of a streamline through a fluid domain indicates its potential for viscous losses; the longer the path taken by a fluid unit as it passes between two points, the less efficient the flow, as that unit has had to pass and irreversibly interact with more fluid before reaching its destination.

Figure 9 shows the results of a goal-oriented analysis, where the real 'cost' associated with a flow feature is assessed by measuring energy loss against progress towards an outlet. Whilst the flow near the walls is expensive in that it produces large irreversible losses, it also provides a return for the invested energy by moving blood quickly from the inlet to the outlet. Two streamlines are compared: B and C, which exit by the same pulmonary artery. In this graph the 'distance from the outlet' is the straight-line distance between a point on the streamline and the exit. The perfect path would be a steep negative gradient indicating a significant reduction of the distance to the outlet as energy is lost. The streamline passing through the 'tight vortex' has sections of positive slope on this graph meaning that it is expending energy but moving away from the outlet. This analysis gives weight to the argument that the recirculations waste energy and should be eliminated by connection design.

Both clinical and numerical investigations have shown that the inclusion of the atrium in the Fontan circuit is detrimental to those factors important for producing and maintaining an acceptable quality of life. Van Haesdonck [11] used numerical simulations in simplified geometry of the APC and TCPC arrangements to conclude that the atrial connection caused significantly greater power losses. The same conclusion was reached by Low *et al.* [6] using rigid *in vitro* models, and by Kim *et al.* [12] with more realistically shaped glass models.

CONCLUSIONS

Volume-based methods for estimating irreversible energy losses or entropy production from CFD solutions have been presented and applied to patient-specific models of Fontan connections. Spatial variation of the viscous dissipation function was used to elucidate how energy was lost in a connection. While inspection of this function indicated that the major losses occur in the wall shear layers there are contributions to energy loss arising from vortices in the collision region between opposing streams. By integrating the viscous dissipation along streamlines the roles of different flow structures were explored. The proposed goal-oriented analysis successfully identifies regions where energy is unnecessarily lost.

NOMENCLATURE

c_p	constant pressure-specific heat, J/kg K
Ec	Eckert number, $U^2/c_p\Delta T$
h	specific enthalpy, J/Kg
k	thermal conductivity, W/mK
L	length scale, m
Nu	Nusselt number, $qL/k\Delta T$
P	pressure, N/m^2
Pr	Prandtl number, v/α
Q	heat transfer, W
$\dot{Q}_{\text{irrev}}$	rate of irreversible heat loss, W
Re	Reynolds number, UL/v
t	time, s
T	temperature, K
U_{ref}	reference velocity, m/s
$\mathbf{u}$	velocity vector, m/s
W	work, W
Φ	viscous dissipation function, 1/s^2
θ	nondimensional temperature, $(T - T_0)/\Delta T$
α	thermal diffusivity, $k/\rho c_p$
ρ	density, kg/m^3
μ	dynamic viscosity, Ns/m^2
v	kinematic viscosity, μ/ρ

ACKNOWLEDGEMENTS

The support of the National Heart Foundation of New Zealand is gratefully acknowledged.

REFERENCES

1. Jones SA. A relationship between Reynolds stresses and viscous dissipation: implications to red cell damage. *Annals of Biomedical Engineering* 1995; **23**(1):21–28.
2. Wooton DM, Ku DN. Fluid mechanics of vascular systems, diseases, and thrombosis. *Annual Review of Biomedical Engineering* 1999; **1**:299–329.
3. Dubini G, de Leval MR, Pietrabissa R, Montevecchi FM, Fumero R. A numerical fluid mechanical study of repaired congenital heart defects: application to the total cavopulmonary connection. *Journal of Biomechanics* 1996; **29**(1):111–121.
4. Guadagni G, Bove EL, Migliavacca F, Dubini G. Effects of pulmonary afterload on the haemodynamics after the Hemi–Fontan procedure. *Medical Imaging and Physics* 2001; **23**:293–298.
5. Sharma SA, Goudy SA, Walker P, Panchal SR, Ensley A, Kanter K, Tam VE, Fyfe D, Yoganathan A. *In vitro* flow experiments for determination of optimal geometry of total cavopulmonary connection for surgical repair of children with functional single ventricle. *Journal of the American College of Cardiology* 1996; **27**(5):1264–1267.
6. Low HT, Chew YT, Lee CN. Flow studies on atriopulmonary and cavopulmonary connections of the Fontan operations for congenital heart defects. *Journal of Biomedical Engineering* 1993; **15**:303–307.
7. Healy TM, Lucas C, Yoganathan AP. Noninvasive fluid dynamic power loss assessments for total cavopulmonary connections using the viscous dissipation function: a feasibility study. *Journal of Biomechanical Engineering* 2001; **123**:317–324.
8. Were CJ. The free-ALE method for unsteady incompressible flow in deforming geometries. *Ph.D. Thesis*, University of Auckland, Auckland, 1996.
9. Leonard BP, Mokhtari S. Beyond first order upwinding: the ULTRA-SHARP alternative for non-oscillatory steady state simulation of convection. *International Journal of Numerical Methods in Engineering* 1990; **30**:729–766.
10. Moyle KR. Haemodynamics of the Fontan connection: investigating patient specific model creation and validation from MRI data. *Ph.D. Thesis*, University of Auckland, Auckland, 2003.
11. van Haesdonck JM, Mertens L, Sizaire R, Montas G, Purnode B, Daenen W, Crochet M, Gewillig M. Comparison by computerized numeric modeling of energy losses in different Fontan connections. *Circulation* 1995; **92**(suppl. II):322–326.
12. Kim YH, Walker PG, Fontaine AA, Panchal S, Ensley AE, Oshinski J, Sharma S, Ha B, Lucas CL, Yoganathan AP. Haemodynamics of the Fontan connection an *in-vitro* study. *Journal of Biomechanical Engineering* 1995; **117**:423–428.

